THE JOURNAL OF PHYSICAL CHEMISTRY Letters

Letter

pubs.acs.org/JPCL

Macroscopic Structural Compositions of π-Conjugated Polymers: Combined Insights from Solid-State NMR and Molecular Dynamics Simulations

Anton Melnyk,[†,‡] Matthias J. N. Junk,[§] Michael D. McGehee,[∥] Bradley F. Chmelka,[§] Michael Ryan Hansen,*[,†,⊥] and Denis Andrienko*[,†]

[†]Max Planck Institute for Polymer Research, Ackermannweg 10, D-55128 Mainz, Germany

[‡]Graduate School Materials Science in Mainz, Staudingerweg 9, D-55128 Mainz, Germany

[§]Department of Chemical Engineering, University of California, Santa Barbara, California 93106, United States

[∥]Department of Materials Science and Engineering, Stanford University, Stanford, California 94305, United States

[⊥]Institute of Physical Chemistry, Westfälische Wilhelms-Universität Münster, Corrensstr. 28/30, D-48149 Münster, Germany

Supporting Information

ABSTRACT: Molecular dynamics simulations are combined with solid-state NMR measurements to gain insight into the macroscopic structural composition of the π-conjugated polymer poly(2,5-bis(3-tetradecyl-thiophen-2-yl)thieno[3,2-*b*]thiophene) (PBTTT). The structural and dynamical properties, as established by the NMR analyses, were used to test the local structure of three constitutient mesophases with (i) crystalline backbones and side chains, (ii) lamellar backbones and disordered side chains, or (iii) amorphous backbones and side chains. The relative compositions of these mesophases were then determined from the deconvolution of the ^{1}H and ^{13}C solid-state NMR spectra and dynamic order parameters. Surprisingly, on the basis of molecular dynamics simulations, the powder composition consisted of only 28% of the completely crystalline mesophase, while 23% was lamellar with disordered side chains and 49% amorphous. The protocol presented in this work is a general approach and can be used for elucidating the relative compositions of mesophases in π-conjugated polymers.

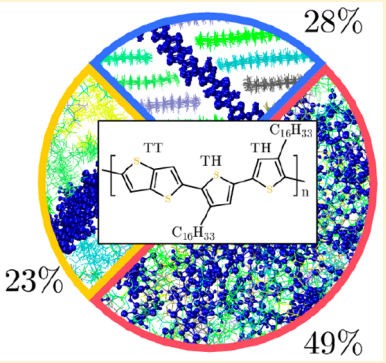

Thiophene-based conjugated polymers are prototypical low-cost materials for solution-processed organic solar cells and thin-film transistors.[1−4] Poly(2,5-bis(3-alkylthiophen-2-yl)thieno[3,2-*b*] thiophene) (PBTTT), the chemical structure of which is shown in Figure 1d, is a typical representative for such polymers. Upon crystallization from a liquid-crystalline phase, pristine PBTTT forms a complex network of ordered and disordered regions with extended crystalline domains.[5] It is often argued that the molecular-scale packing of PBTTT[6−15] accounts for its high charge carrier mobility, up to 1 cm^2/(V s), as measured in thin-film transistors.[7,16−19]

Despite their technological importance, morphology−mobility relations of π-conjugated polymers are still difficult to establish. Counterintuitively, a higher degree of crystallinity does not necessarily lead to an increase in charge-carrier mobility.[20] In many cases, such relations cannot be formulated because the detailed atomic structure is challenging to determine from standard experimental techniques alone. In these soft matter systems, entropic effects and lack of long-range order limit the information that can be obtained from scattering techniques, such as X-ray diffraction. Spectroscopic and microscopy techniques do provide information about local ordering,[21−24] however, only as macroscopic averages over all mesophases present in the sample. For example, solid-state NMR spectroscopy can be an appropriate tool to infer local structural motifs of organic materials,[25−28] in addition to being sensitive to conformational effects and chain dynamics.[29,30] Here, we show that it is possible to resolve the macroscopic structural composition of a π-conjugated polymer (PBTTT-C_{16}) by combining solid-state NMR analyses with molecular dynamics simulations, in a manner that is analogous to what has been achieved recently using inelastic neutron scattering for doped P3HT.[31]

The local ordering of polymer backbones in the sample can be quantitatively determined by analyses of solid-state one-dimensional (1D) single-pulse ^{1}H magic-angle-spinning (MAS) NMR spectra. For example, the spectrum in Figure 2a shows resolved resonances around 6−7 ppm from two types of aromatic protons on the π-conjugated backbone (shown in green and blue in Figure 1d, top). This signal indeed consists of two distinct contributions (cyan and blue curves in Figure 2a), with maxima at 6.9 and 6.1 ppm and relative integrated signal intensities of 0.49 and 0.51, respectively. In solution, these aromatic protons give rise to isotropic ^{1}H chemical shifts of 7.15 and 7.30 ppm (Figure S1). The fact that the aromatic ^{1}H

Received: June 7, 2017
Accepted: August 15, 2017
Published: August 15, 2017

DOI: 10.1021/acs.jpclett.7b01443
J. Phys. Chem. Lett. 2017, 8, 4155−4160

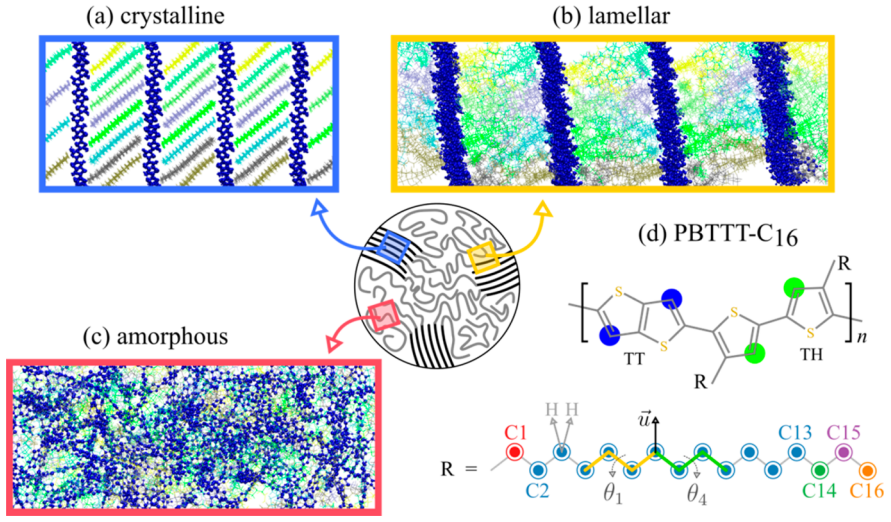

Figure 1. Model mesophases of PBTTT-C_{16}: (a) crystalline, (b) lamellar, and (c) amorphous. (d) Chemical structure of PBTTT-C_{16} and atom labeling used in this study. $\vec{u}$ is a unit vector that defines the orientation of the CH_2 group, and the angles θ_1 and θ_4 identify the local environment of a CH_2 moiety to account for the γ-gauche effect.

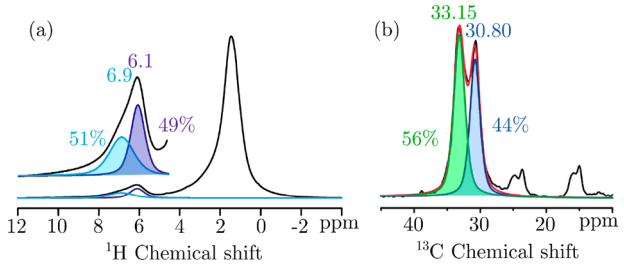

Figure 2. (a) Solid-state ^{1}H MAS NMR spectrum of PBTTT-C_{16} recorded at room temperature under MAS conditions of 29.7 kHz. Optimized fits of the two aromatic contributions at 6.1 and 6.9 ppm are depicted in blue and cyan, respectively. (b) Single-pulse solid-state ^{13}C MAS NMR spectrum (black) recorded at 298 K with a MAS frequency of 12.5 kHz. The optimized fits of the dominant methylene ^{13}C signals at 33.15 and 30.80 ppm are shown in green and blue, respectively, to yield the combined spectral fit (red).

signal at 6.1 ppm is displaced by ~1.2 ppm shows that these protons are strongly influenced by nuclear shielding effects associated with $\pi-\pi$ stacking of the aromatic polymer backbones. In contrast, the aromatic ^{1}H signal at 6.9 ppm is displaced by only 0.2 ppm, demonstrating that this signal is not exposed to significant $\pi-\pi$ shielding effects. These observations are consistent with the two ^{1}H signals at 6.9 and 6.1 ppm being assigned to disordered and ordered backbone moieties, respectively, where each ^{1}H signal is a sum of signals from the thiophene (TT) and thienothiophene (TH) groups. Hence, we conclude that the fractions of ordered (π-stacked) and disordered backbones are 0.49 and 0.51, respectively.

Apart from the backbone conformations, the composition of the PBTTT-C_{16} sample can be elucidated from the conformational statistics of the C_{16} side chains. In solid-state NMR, these statistics can be assessed through the γ-gauche effect:[32] higher frequencies are detected if two CH_2 groups are in a relative γ-position to one another (*trans/trans*, *tt*), whereas lower frequencies for the *trans/gauche* (*tg*) and *gauche/gauche* (*gg*) conformations are expected. To quantitatively determine the fractions of *tt*, *tg*, and *gg* conformations, a single-pulse solid-state ^{13}C MAS NMR spectrum was acquired with high-power ^{1}H decoupling during acquisition and a recycle delay of 10 s, corresponding to ~5T_1. The resulting single-pulse ^{13}C MAS spectrum of the alkyl region in Figure 2b exhibits two peaks at 33.15 and 30.80 ppm associated with the C_{16} side chains, which are assigned to *tt* and either of the less ordered *tg* or *gg* conformers, respectively. The resulting integrated intensities enable the relative conformer fractions to be determined, with the *tt* conformations accounting for 56% of the overall signal intensity, while 44% arises from the *tg* and *gg* conformations.

These conformations, however, do not directly represent the fractions of crystalline and amorphous domains in the sample, as has often been assumed, for example, for semicrystalline polyhydrocarbons.[33−35] While the crystallites of PBTTT indeed have C_{16} side chains predominantly in the *tt* state, the disordered mesophases have C_{16} side chains that include both *tt* and *tg* + *gg* conformers, which contribute to both ^{13}C resonances in the spectrum. Thus, to determine the structural composition, we assume that three mesophases are present in the material: crystalline (c), lamellar (l), and amorphous (a), as shown in Figure 1a−c, where lamellar refers more specifically to π-stacked backbones and disordered side chains. Because every mesophase has its own fraction of *tt*, *tg*, and *gg* conformers, f_c^{tt}, f_l^{tt}, and f_a^{tt}, the NMR signal from a powdered sample is the sum of these fractions weighted by the mesophase number fractions, n_c, n_l, and n_a:

$$f_c^{tt} n_c + f_l^{tt} n_l + f_a^{tt} n_a = f_{NMR}^{tt} \quad (1)$$

$$n_c + n_l + n_a = 1 \quad (2)$$

Similar relations hold for the *tg* and *gg* conformations. The second equation is the normalization condition for the mesophase number fractions. Unfortunately, the fractions f_c^{tt}, f_l^{tt}, and f_a^{tt} cannot be accessed directly, because it has so far not been possible to prepare a π-conjugated polymer sample containing a specific mesophase only. However, this is straightforward to do using computer simulations. The three mesophases were each modeled using molecular dynamics simulations of 128 PBTTT-C_{16} polymer chains, as detailed in the Supporting Information. Representative snapshots are shown in Figure 1a−c. The classification of configurations into *tt*, *tg*, and *gg* states was achieved via discrete partitioning of two dihedral angles, θ_1 and θ_4 (Figure 1d), attached to the

DOI: 10.1021/acs.jpclett.7b01443
J. Phys. Chem. Lett. 2017, 8, 4155−4160

moiety of interest. Further details concerning the partitioning of *tt*, *tg*, and *gg* states are given in the Supporting Information.

The fractions of the *tt* and *tg*+*gg* conformations in the PBTTT material, as determined from molecular dynamics, are listed in Table 1. As expected, the C_{16} side chains are predominantly in the *tt* state for the crystalline mesophase. Interestingly, the partitioning of *tt* and *tg*+*gg* states is similar for the C_{16} side chains in the lamellar and amorphous mesophases. Thus, we assume in the following $f_l^{tt} \approx f_a^{tt}$. Substituting the values of simulated fractions into eq 1, we obtain $n_c = 0.28$ and $n_a + n_l = 0.72$. To distinguish between amorphous and lamellar mesophases, we utilize the fact that the intermolecular separations between backbones in crystalline and lamellar domains are expected to be similar (see the Supporting Information for details) and contribute to one peak in the solid-state ^{13}C MAS NMR spectrum only (see Figure 2b). Hence, $n_c + n_l = 0.49$; therefore, $n_l = 0.21$ and $n_a = 0.51$. This is a remarkable result: our calculations suggest that only 28% of the system is in a true crystalline state, in which both the C_{16} side chains and PBTTT backbones are ordered. The remaining part of the sample is either in the lamellar (21%) or amorphous (51%) mesophases. Had we assumed that we have only two mesophases (amorphous and crystalline), the C_{16} side chain statistics would have predicted that the fraction of the crystalline phase is 28% ($n_l = 0$), which is inconsistent with the value of 49% from ^1H MAS NMR for the PBTTT backbone. Thus, it is essential to account for the lamellar mesophase presence in a π-conjugated polymer in order to interpret properly the solid-state NMR results.

Table 1. Simulated and Measured Fractions of *tt* and *tg* + *gg* Conformers and *tt*-Resolved Dynamic Order Parameters in the Crystalline, Lamellar, and Amorphous Mesophases

	crystalline	lamellar	amorphous	sample (NMR)
f^{tt}	0.95	0.41	0.39	0.56
f^{tg+gg}	0.05	0.59	0.61	0.44
S^{tt}	0.83	0.46	0.49	0.71

Apart from the statistics for the C_{16} side chain and PBTTT backbone conformations, solid-state NMR can also provide access to the dynamic order parameters,[30] or equivalently the relative number of microstates visited by a specific bond vector during an NMR measurement. Here, we have employed the 2D $^{13}C\{^1H\}$ rotor-encoded rotational-echo double resonance (REREDOR) and rotor-encoded polarization transfer heteronuclear dipolar-order (REPT-HDOR) experiments to evaluate the one-bond $^1H-^{13}C$ order parameters. While the dipolar coupling constant (D_{CH}) of a rigid −CH− group is 21.0 kHz,[36] any rotational motion faster than the NMR time scale (>μs) partially averages the $^1H-^{13}C$ dipole−dipole coupling (DDC) and hence decreases D_{CH}. This enables determination of a dynamic order parameter S_{NMR} by dividing the experimentally measured value D_{CH} by the theoretical value for a fully rigid $-CH_n-$ group, $S_{NMR} = D_{exp}/D_{rigid}$. Values of S_{NMR} range from 0 to 1, where values closer to unity correspond to greater local rigidity. The resulting rotor-encoded $^1H-^{13}C$ dipole−dipole sideband patterns are shown in Figure 3a,c. The $^1H-^{13}C$ DDCs were obtained by a spectral fitting procedure that accounts for the strong DDC contribution of the directly bonded $-CH_n-$ (n = 1−3) moieties and an additional weak background contribution due to couplings with remote protons.

The results provide insight into site-selective rotational dynamics of the main-chain and alkyl side chains in PBTTT-C16: For the ordered PBTTT backbone, corresponding to the crystalline and lamellar PBTTT regions, the analysis leads to mean DDCs of 19.6 kHz and 18.7 kHz for the −CH− groups of the thienothiophene and thiophene rings, respectively. Both DCCs are close to 21.0 kHz with S_{NMR} being around ∼0.9, corresponding to a fairly rigid −CH− moiety. Hence, the well-ordered $\pi-\pi$-stacking arrangement in PBTTT-C_{16} only allows the aromatic backbone to experience minor dynamic reorientations on the approximately microsecond NMR time scale most likely associated with small out-of-plane fluctuations. Insufficient signal intensity prevented a detailed analysis of the

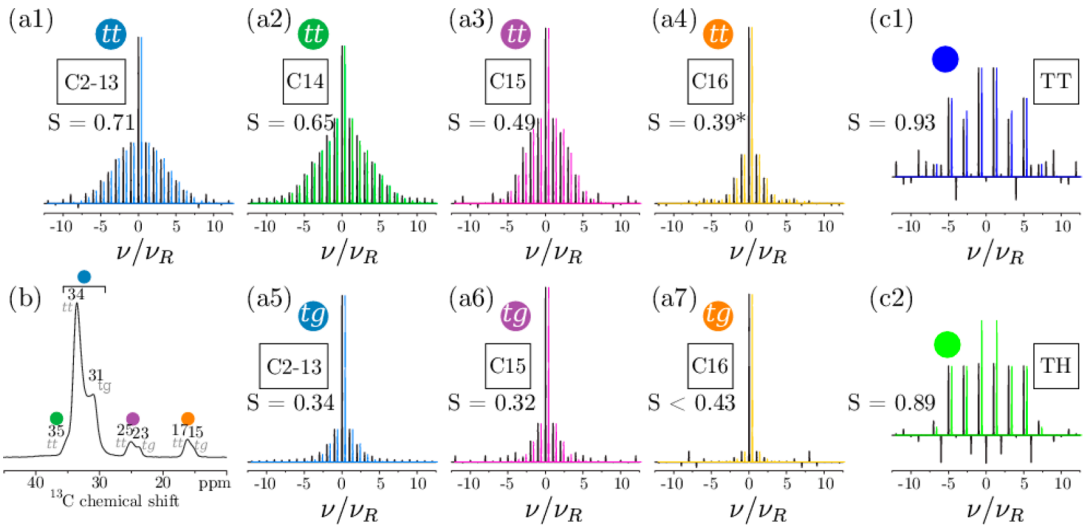

Figure 3. (a1−a7) Experimental *tt*/*tg* + *gg*-resolved 1D $^{13}C\{^1H\}$ REREDOR dipolar sideband patterns (black) and corresponding fits (color) for all spectrally distinct ^{13}C moieties of the C_{16} side chain. Here, *tg* is used to denote *tg*+*gg*. (b) ^{13}C chemical shifts in the $^{13}C\{^1H\}$ CP/MAS NMR spectrum. (c1, c2) Experimental $^{13}C\{^1H\}$ REPT-HDOR dipole−dipole sideband patterns (black) and corresponding fits (color) for proton-bearing ^{13}C moieties of the thiophene (TH) and thienothiophene (TT) groups of the PBTTT polymer backbone. Numbering and coloring correspond to the scheme given in Figure 1d.

DOI: 10.1021/acs.jpclett.7b01443
J. Phys. Chem. Lett. 2017, 8, 4155−4160

dipolar coupling constants at ^{13}C spectral positions corresponding to the −CH− moieties of disordered $\pi-\pi$ stacks (see Figure S2).

A mean D_{CH} value of 14.9 kHz was determined for the central methylene groups of the C_{16} side chains in the *tt* conformation (see Figure 3a1). While this part of the alkyl chain is fairly rigid with $S_{NMR} \sim 0.71$, the S_{NMR} values are lower (0.65, 0.49, and 0.39) for the last three methylene and methyl groups of the C_{16} side chains in the *tt* conformation (see Figure 3a2−a4). It is surprising that both structural and dynamic ordering prevail up to the terminal $-CH_3$ group for side chains composed of as many as 16 structural units. For all ^{13}C moieties of the C_{16} side chains in *gauche* conformations, the D_{CH} values are considerably smaller than their counterparts in *tt* conformations. For example, D_{CH} values of the central methylene groups decrease by more than a factor of 2, yielding an S_{NMR} value as low as 0.34 (see Figure 3a5−a7). Similar values of 0.32 and <0.4 are obtained for the terminal methylene and methyl moieties. Hence, the decrease in structural order of the C_{16} side chains with *gauche* conformations is manifested by a considerable increase in segmental rotational mobility.

Similar to the statistics of *tt* and *tg* + *gg* states, dynamic order parameters can be used to determine (or refine) the macroscopic structural composition of the sample. To do this, we have evaluated the dynamic order parameter, S_{MD}, as the long-time limit of an autocorrelation function (ACF)[37,38]

$$S_{MD}^2 = \lim_{t\to\infty} \langle P_2(\vec{u}(t_0)\cdot\vec{u}(t))\rangle \quad (3)$$

Here, $\vec{u}(t)$ is the unit vector along the $-CH_2-$ moiety in the alkyl chain as illustrated in Figure 1d, and P_2 is the second Legendre polynomial; the average $\langle ... \rangle$ is preformed over initial times t_0 and the ensemble of equivalent $-CH_2-$ groups (64 backbones and 512 C_{16} side chains). S_{MD} for backbone $-CH_2-$ groups were determined to be 0.96, 0.93, and 0.83 in the crystalline, lamellar, and amorphous mesophases, respectively. The first two values (experimental data for amorphous backbones are not available) compare well to the measured values of 0.9, confirming that the PBTTT backbones are rather immobile, at least on a microsecond time scale. For the C_{16} side chains, the γ-gauche effect can be used to differentiate between the *tt*- and *tg* + *gg*-conformers. In the MD simulations, we do this by following the dynamics of θ_1 and θ_4 dihedral angles, which are shown in Figure 1d, and assign every $-CH_2-$ group to one of the states *tt* or *tg* + *gg*. S_{MD} is then evaluated for every state and $-CH_2-$ group. As anticipated, interdigitated crystalline C_{16} side chains in the *tt* state have higher S_{MD}^{tt} values in the range 0.74−0.88 than the corresponding disordered C_{16} side chains of lamellar and amorphous mesophases (S_{MD}^{tt} = 0.33−0.60), in qualitative agreement with previous works.[14,15] Note that the fraction of *tg* + *gg* conformers is too small (about 5%) to evaluate their S_{MD} in the crystalline mesophase (see the Supporting Information for details).

We can now use the calculated S_{MD} to refine the sample's composition. To do this, we complement eq 1 with an equation for the dynamic order parameter S_{NMR} for the *tt* states only:

$$S_{MD,c}^{tt} n_c + S_{MD,l}^{tt} n_l + S_{MD,a}^{tt} n_a = S_{NMR}^{tt} \quad (4)$$

Solving eqs 1, 2, and 4 (see the Supporting Information) yields n_c = 0.28, n_l = 0.23, and n_a = 0.49. Remarkably, these equations contain information about the C_{16} side chains only, yet they give values consistent with the PBTTT backbone solid-state NMR data, namely, n_a = 0.51 and $n_c + n_l$ = 0.49. The composition of a crystalline PBTTT-C_{16} powdered sample can therefore be deduced from either the static or dynamic properties of alkyl side chains and backbones.

For the present case of PBTTT-C_{16}, the ordered fraction of PBTTT backbones accounts for 51% of the powdered sample with $S_{NMR/MD}$ of 0.90. As measured from the entire sample, the alkyl side chains have fractions of 0.54 (*tt*) and 0.46 (*tg* + *gg*) with S_{NMR} of 0.71 (*tt*) and 0.34 (*tg* + *gg*) for the inner carbons. Complementing these measurements with MD simulations of crystalline, lamellar, and amorphous mesophases, we are able to elucidate the structural composition of the entire powdered PBTTT-C_{16} sample. In particular, the MD simulations reveal that the crystalline and lamellar mesophases account for 28% and 23%, respectively, while 49% of the sample is amorphous. Our study clearly shows that the interpretation of experimental data requires a model that accounts for the local molecular packing, as well as mesoscopic structural composition of a material. The strategy presented in this work is expected to be general and useful for quantitative analyses of the structural compositions of similar π-conjugated polymer materials.

■ ASSOCIATED CONTENT

Supporting Information

The Supporting Information is available free of charge on the ACS Publications website at DOI: 10.1021/acs.jpclett.7b01443.

Details of molecular dynamics simulations, solid-state NMR experimental details, and the solution-state NMR spectrum (PDF)

■ AUTHOR INFORMATION

Corresponding Authors

*E-mail: mhansen@uni-muenster.de.
*E-mail: denis.andrienko@mpip-mainz.mpg.de.

ORCID

Michael D. McGehee: 0000-0001-9609-9030
Bradley F. Chmelka: 0000-0002-4450-6949
Michael Ryan Hansen: 0000-0001-7114-8051
Denis Andrienko: 0000-0002-1541-1377

Notes

The authors declare no competing financial interest.

■ ACKNOWLEDGMENTS

We are grateful to Prof. Ian McCulloch for providing the PBTTT-C_{16} material. The work at MPIP was supported by the BMBF project MEDOS (FKZ 03EK3503B), MESOMERIE (FKZ 13N10723), and INTERPHASE (FKZ 13N13657) as well as the NMP-20-2014: Widening materials models program (project MOSTOPHOS, Grant 646259). The work at UCSB was supported by the Institute for Collaborative Biotechnologies through Grant W911NF-09-0001 from the USARO. M.R.H. acknowledges financial support from the Villum Foundation, Denmark, under the Young Investigator Programme (VKR023122). A.M. thanks C. Poelking, A. Fogarty, J. Rudzinski, C. Greco, T. Bereau, and R. Potestio for helpful discussions and acknowledges the financial support from graduate school MAINZ as a recipient of the fellowship through the Excellence Initiative (DFG/GSC 266). M.J.N.J. acknowledges financial support from the Alexander von Humboldt-Foundation through a Feodor Lynen Research Fellowship.

DOI: 10.1021/acs.jpclett.7b01443
J. Phys. Chem. Lett. 2017, 8, 4155−4160

REFERENCES

(1) McCullough, R. D. The Chemistry of Conducting Polythiophenes. *Adv. Mater.* **1998**, *10* (2), 93−116.

(2) McCulloch, I.; Heeney, M.; Chabinyc, M. L.; DeLongchamp, D.; Kline, R. J.; Coelle, M.; Duffy, W.; Fischer, D.; Gundlach, D.; Hamadani, B.; et al. Semiconducting Thienothiophene Copolymers: Design, Synthesis, Morphology, and Performance in Thin-Film Organic Transistors. *Adv. Mater.* **2009**, *21* (10−11), 1091−1109.

(3) Boudreault, P.-L. T.; Najari, A.; Leclerc, M. Processable Low-Bandgap Polymers for Photovoltaic Applications. *Chem. Mater.* **2011**, *23* (3), 456−469.

(4) McCulloch, I.; Ashraf, R. S.; Biniek, L.; Bronstein, H.; Combe, C.; Donaghey, J. E.; James, D. I.; Nielsen, C. B.; Schroeder, B. C.; Zhang, W. Design of Semiconducting Indacenodithiophene Polymers for High Performance Transistors and Solar Cells. *Acc. Chem. Res.* **2012**, *45* (5), 714−722.

(5) Schuettfort, T.; Watts, B.; Thomsen, L.; Lee, M.; Sirringhaus, H.; McNeill, C. R. Microstructure of Polycrystalline PBTTT Films: Domain Mapping and Structure Formation. *ACS Nano* **2012**, *6* (2), 1849−1864.

(6) McCulloch, I.; Heeney, M.; Bailey, C.; Genevicius, K.; MacDonald, I.; Shkunov, M.; Sparrowe, D.; Tierney, S.; Wagner, R.; Zhang, W.; et al. Liquid-Crystalline Semiconducting Polymers with High Charge-Carrier Mobility. *Nat. Mater.* **2006**, *5* (4), 328−333.

(7) Chabinyc, M. L.; Toney, M. F.; Kline, R. J.; McCulloch, I.; Heeney, M. X-Ray Scattering Study of Thin Films of Poly(2,5-Bis(3-Alkylthiophen-2-Yl)Thieno[3,2-b]Thiophene. *J. Am. Chem. Soc.* **2007**, *129* (11), 3226−3237.

(8) DeLongchamp, D. M.; Kline, R. J.; Lin, E. K.; Fischer, D. A.; Richter, L. J.; Lucas, L. A.; Heeney, M.; McCulloch, I.; Northrup, J. E. High Carrier Mobility Polythiophene Thin Films: Structure Determination by Experiment and Theory. *Adv. Mater.* **2007**, *19* (6), 833−837.

(9) Northrup, J. E. Atomic and Electronic Structure of Polymer Organic Semiconductors: P3HT, PQT, and PBTTT. *Phys. Rev. B: Condens. Matter Mater. Phys.* **2007**, *76* (24), 245202.

(10) Brocorens, P.; Van Vooren, A.; Chabinyc, M. L.; Toney, M. F.; Shkunov, M.; Heeney, M.; McCulloch, I.; Cornil, J.; Lazzaroni, R. Solid-State Supramolecular Organization of Polythiophene Chains Containing Thienothiophene Units. *Adv. Mater.* **2009**, *21* (10−11), 1193−1198.

(11) DeLongchamp, D. M.; Kline, R. J.; Jung, Y.; Germack, D. S.; Lin, E. K.; Moad, A. J.; Richter, L. J.; Toney, M. F.; Heeney, M.; McCulloch, I. Controlling the Orientation of Terraced Nanoscale "Ribbons" of a Poly(Thiophene) Semiconductor. *ACS Nano* **2009**, *3* (4), 780−787.

(12) Cho, E.; Risko, C.; Kim, D.; Gysel, R.; Cates Miller, N.; Breiby, D. W.; McGehee, M. D.; Toney, M. F.; Kline, R. J.; Bredas, J.-L. Three-Dimensional Packing Structure and Electronic Properties of Biaxially Oriented Poly(2,5-Bis(3-Alkylthiophene-2-Yl)Thieno[3,2-b]-Thiophene) Films. *J. Am. Chem. Soc.* **2012**, *134* (14), 6177−6190.

(13) Rivnay, J.; Noriega, R.; Northrup, J. E.; Kline, R. J.; Toney, M. F.; Salleo, A. Structural Origin of Gap States in Semicrystalline Polymers and the Implications for Charge Transport. *Phys. Rev. B: Condens. Matter Mater. Phys.* **2011**, *83* (12), 121306.

(14) Alberga, D.; Mangiatordi, G. F.; Torsi, L.; Lattanzi, G. Effects of Annealing and Residual Solvents on Amorphous P3HT and PBTTT Films. *J. Phys. Chem. C* **2014**, *118* (16), 8641−8655.

(15) Alberga, D.; Perrier, A.; Ciofini, I.; Felice Mangiatordi, G.; Lattanzi, G.; Adamo, C. Morphological and Charge Transport Properties of Amorphous and Crystalline P3HT and PBTTT: Insights from Theory. *Phys. Chem. Chem. Phys.* **2015**, *17* (28), 18742−18750.

(16) Hamadani, B. H.; Gundlach, D. J.; McCulloch, I.; Heeney, M. Undoped Polythiophene Field-Effect Transistors with Mobility of 1 Cm(2) V(−1) s(−1). *Appl. Phys. Lett.* **2007**, *91* (24), 243512.

(17) Umeda, T.; Kumaki, D.; Tokito, S. Surface-Energy-Dependent Field-Effect Mobilities up to 1 Cm2/V s for Polymer Thin-Film Transistor. *J. Appl. Phys.* **2009**, *105* (2), 024516−024516−5.

(18) Lee, M. J.; Gupta, D.; Zhao, N.; Heeney, M.; McCulloch, I.; Sirringhaus, H. Anisotropy of Charge Transport in a Uniaxially Aligned and Chain-Extended, High-Mobility, Conjugated Polymer Semiconductor. *Adv. Funct. Mater.* **2011**, *21* (5), 932−940.

(19) Wang, C.; Jimison, L. H.; Goris, L.; McCulloch, I.; Heeney, M.; Ziegler, A.; Salleo, A. Microstructural Origin of High Mobility in High-Performance Poly(Thieno-Thiophene) Thin-Film Transistors. *Adv. Mater.* **2010**, *22* (6), 697−701.

(20) Noriega, R.; Rivnay, J.; Vandewal, K.; Koch, F. P. V.; Stingelin, N.; Smith, P.; Toney, M. F.; Salleo, A. A General Relationship between Disorder, Aggregation and Charge Transport in Conjugated Polymers. *Nat. Mater.* **2013**, *12* (11), 1038−1044.

(21) Rahaman, M. H. A.; Uddin Khandaker, M.; Raza Khan, Z.; Zieauddin Kufian, M.; Mohd Noor, I. S.; Kariem Arof, A. Effect of Gamma Irradiation on Poly(Vinyledene Difluoride)−lithium Bis-(Oxalato)Borate Electrolyte. *Phys. Chem. Chem. Phys.* **2014**, *16* (23), 11527−11537.

(22) Snyder, C. R.; Nieuwendaal, R. C.; DeLongchamp, D. M.; Luscombe, C. K.; Sista, P.; Boyd, S. D. Quantifying Crystallinity in High Molar Mass Poly(3-Hexylthiophene). *Macromolecules* **2014**, *47* (12), 3942−3950.

(23) Gao, X.; Wang, L.; Luo, H.; Zou, Q.; Feng, N.; Feng, J. Crystalline Phases in Ethylene Copolymers Studied by Solid-State NMR and DSC. *Macromolecules* **2010**, *43* (13), 5713−5722.

(24) Shen, X.; Hu, W.; Russell, T. P. Measuring the Degree of Crystallinity in Semicrystalline Regioregular Poly(3-Hexylthiophene). *Macromolecules* **2016**, *49* (12), 4501−4509.

(25) May, F.; Marcon, V.; Hansen, M. R.; Grozema, F.; Andrienko, D. Relationship between Supramolecular Assembly and Charge-Carrier Mobility in Perylenediimide Derivatives: The Impact of Side Chains. *J. Mater. Chem.* **2011**, *21* (26), 9538−9545.

(26) Feng, X.; Marcon, V.; Pisula, W.; Hansen, M. R.; Kirkpatrick, J.; Grozema, F.; Andrienko, D.; Kremer, K.; Müllen, K. Towards High Charge-Carrier Mobilities by Rational Design of the Shape and Periphery of Discotics. *Nat. Mater.* **2009**, *8* (5), 421−426.

(27) Etzold, F.; Howard, I. A.; Forler, N.; Melnyk, A.; Andrienko, D.; Hansen, M. R.; Laquai, F. Sub-Ns Triplet State Formation by Non-Geminate Recombination in PSBTBT:PC70BM and PCPDTBT:PC60BM Organic Solar Cells. *Energy Environ. Sci.* **2015**, *8* (5), 1511−1522.

(28) Hansen, M. R.; Graf, R.; Spiess, H. W. Interplay of Structure and Dynamics in Functional Macromolecular and Supramolecular Systems As Revealed by Magnetic Resonance Spectroscopy. *Chem. Rev.* **2016**, *116* (3), 1272−1308.

(29) Tonelli, A. E.; Schilling, F. C. Carbon-13 NMR Chemical Shifts and the Microstructure of Polymers. *Acc. Chem. Res.* **1981**, *14* (8), 233−238.

(30) Hansen, M. R.; Graf, R.; Spiess, H. W. Solid-State NMR in Macromolecular Systems: Insights on How Molecular Entities Move. *Acc. Chem. Res.* **2013**, *46* (9), 1996−2007.

(31) Harrelson, T. F.; Cheng, Y. Q.; Li, J.; Jacobs, I. E.; Ramirez-Cuesta, A. J.; Faller, R.; Moulé, A. J. Identifying Atomic Scale Structure in Undoped/Doped Semicrystalline P3HT Using Inelastic Neutron Scattering. *Macromolecules* **2017**, *50* (6), 2424−2435.

(32) Born, R.; Spiess, H. W. Conformational Effects and Configurational Splitting in 13C NMR Spectra of Synthetic Polymers As Investigated by Ab Initio Individual Gauges for Localized Molecular Orbitals (IGLO) Calculations. *Macromolecules* **1995**, *28* (23), 7785−7795.

(33) Siu, S. W. I.; Pluhackova, K.; Böckmann, R. A. Optimization of the OPLS-AA Force Field for Long Hydrocarbons. *J. Chem. Theory Comput.* **2012**, *8* (4), 1459−1470.

(34) Casal, H. L.; Mantsch, H. H. Positional Dependence of Solvent Effects on the Conformation of Liquid N-Alkanes. An Infrared Spectroscopic Study. *J. Mol. Struct.* **1989**, *192* (1), 41−45.

(35) Snyder, R. G.; Poore, M. W. Conformational Structure of Polyethylene Chains from the Infrared Spectrum of the Partially Deuterated Polymer. *Macromolecules* **1973**, *6* (5), 708−715.

DOI: 10.1021/acs.jpclett.7b01443
J. Phys. Chem. Lett. 2017, 8, 4155−4160

(36) Saalwächter, K.; Schnell, I. REDOR-Based Heteronuclear Dipolar Correlation Experiments in Multi-Spin Systems: Rotor-Encoding, Directing, and Multiple Distance and Angle Determination. *Solid State Nucl. Magn. Reson.* **2002**, *22* (2), 154−187.
(37) Lipari, G.; Szabo, A. Model-Free Approach to the Interpretation of Nuclear Magnetic Resonance Relaxation in Macromolecules. 1. Theory and Range of Validity. *J. Am. Chem. Soc.* **1982**, *104* (17), 4546−4559.
(38) Lipari, G.; Szabo, A. Model-Free Approach to the Interpretation of Nuclear Magnetic Resonance Relaxation in Macromolecules. 2. Analysis of Experimental Results. *J. Am. Chem. Soc.* **1982**, *104* (17), 4559−4570.

DOI: 10.1021/acs.jpclett.7b01443
J. Phys. Chem. Lett. 2017, 8, 4155−4160